Accepted Manuscript

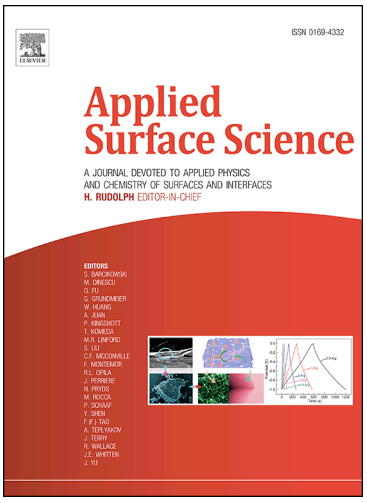

Full Length Article

Study on electronic and optical properties of the twisted and strained MoS_2/PtS_2 heterogeneous interface

Shuo Deng, Yan Zhang, Lijie Li

PII: S0169-4332(19)30112-6
DOI: https://doi.org/10.1016/j.apsusc.2019.01.097
Reference: APSUSC 41496

To appear in: *Applied Surface Science*

Received Date: 8 November 2018
Revised Date: 7 January 2019
Accepted Date: 12 January 2019

Please cite this article as: S. Deng, Y. Zhang, L. Li, Study on electronic and optical properties of the twisted and strained MoS_2/PtS_2 heterogeneous interface, *Applied Surface Science* (2019), doi: https://doi.org/10.1016/j.apsusc.2019.01.097

Study on electronic and optical properties of the twisted and strained MoS_2/PtS_2 heterogeneous interface

Shuo Deng[1, 3], Yan Zhang[2*], and Lijie Li[3*]

[1]School of Logistic Engineering, Wuhan University of Technology, Wuhan 430070, China

[2]School of Physics, University of Electronic Science and Technology of China, Chengdu 610054, China

[3]College of Engineering, Swansea University, Swansea SA1 8EN, UK

[*]Emails: zhangyan@uestc.edu.cn, L.Li@swansea.ac.uk

Abstract

We report electronic and optical properties of the MoS_2/PtS_2 heterogeneous interfaces subject to various twisting angles based on the first principles simulation. In order to sustain the structural stability and avoid to have a large size cell, the optimized rotation angles of the MoS_2/PtS_2 heterogeneous interfaces are 19.1°, 30.0° and 40.9°. It is found from the first principle simulation that the absolute passband amplitude of the refractive index, extinction coefficient, reflectivity and absorption coefficient curves under 30.0° rotation angle are 6-12 times higher than 19.1° and 40.9° rotation angles of the MoS_2/PtS_2 heterogeneous interfaces. Moreover, under the 30.0° twisting angle, the absorption coefficient in the absorption spectrum can reach to or above 10^5/cm. The absorption spectrum has a red-shift and a broadening effect with the tensile strain, from roughly 700 nm (0% externally strain) to 1050 nm (5% externally strain). The prominent optical properties of MoS_2/PtS_2 heterogeneous interface under 30° rotation angle still exist after taking into consideration the spin-orbit coupling (SOC) effect. These results suggest that the MoS_2/PtS_2 heterogeneous interfaces will have great potential applications in tunable optoelectronic devices.

Keywords: MoS_2/PtS_2 heterogeneous structure, twisting angle, strain engineering, optical performance

1. Introduction

As superior properties of two-dimensional (2D) materials have been revealed continuously over the past decade, growing interests have been spurred to investigate

the novel properties and special structures of transition-metal dichalcogenides (TMDs)[1-7] and noble-transition-metal dichalcogenides (nTMDs)[8-13]. Previous theoretical and experimental studies have already predicted that twisting bilayer structures can lead to new devices exhibiting improved electronic properties. For example, a near 1.1^{o} twisted graphene sheets show an unconventional superconductivity in 2D superlattices[5, 14], a mirrored Dirac cones are observed in the 30^{o} twisted bilayer graphene[15, 16]. The van der Waals (vdW) interaction is reported to affect the electronic properties of twisted MX_2/MoS_2 heterogeneous interfaces[17, 18], and the PdS_2 (PtS_2)/grapheme heterogeneous interfaces have been confirmed by the quasi-ohmic contact with twisting angles[19].

Despite that experimentally it is very difficult to achieve a layered structure with a uniform stacking order, various interlayer orientation angles can be obtained with different deposition processes[20]. For example, the twisted MoS_2/WSe_2 heterogeneous interfaces and bilayer graphene have been direct grown[15, 16, 21]. The various twisting angles have been produced by artificially stacking monolayer materials. Recently, Yuan et al. created a twisted multi-layer structure by stacking two graphene sheets with a near 1.1^{o} twisting angle[5, 14]. The top and bottom layers of graphene are originated from the same exfoliated flake, which allows for a precise twisting angle controlled from 0.1^{o} to 0.2^{o}. Although there have been tremendous theoretical and experimental efforts reported the interlayer rotation that can affect the electrical properties, the influence of the interlayer rotation on the optical properties is still unclear, especially in the TMDs/nTMDs heterogeneous interfaces.

In this work, we design and analyze electronic and optical properties of twisted MoS_2/PtS_2 heterogeneous interfaces by the first principle methods, which has been widely used in many previous studies for bilayer structures[14, 17-19, 21-24]. Although some research groups have theoretically analyzed the optical properties of the different heterogeneous interfaces, there is a lack of analysis for twisted heterogeneous interfaces[22-24]. In this paper, our aim is to theoretically explore the effect of parallel twisting for MoS_2/PtS_2 heterogeneous interfaces. For this bilayer structure, the maximum strain of lattice mismatch is calculated to be 1.29%. We calculated that the fluctuation ranges of the optical properties under 30.0^{o} rotation

angle are 6-12 times higher than 19.1° and 40.9° rotation angles. More important, under the 30.0° twisting angles, the absorption coefficient spectrum has a large red-shift range (350 nm) under 0 to 5% external tensile strain and high absorption coefficient is shown to near infrared under 5% external tensile strain.

2 Computational method

The twisted bilayers were calculated using the Generalized Lattice Match (GLM) method[25], which is for calculating the relationship between number of atoms and mismatch strain. We generate the optimized twisting angles by selecting the smaller number of atoms and the mismatch strain. In the GLM method, the rotation angle of monolayer MoS_2 relative to monolayer PtS_2 is defined by the angle between the two zigzag directions. In the Figure 1(a), the surface cell of monolayer MoS_2 crystal is defined by vectors $\mathbf{u}_1$ and $\mathbf{u}_2$, where $\mathbf{u}_1=[u_{1x}, u_{1y}]^T$. In the Figure 1(b), the surface cell of monolayer PtS_2 is defined by vectors $\mathbf{v}_1$ and $\mathbf{v}_2$. Then, the linear equation of [$\mathbf{u}_1$, $\mathbf{u}_2$] and [$\mathbf{v}_1$, $\mathbf{v}_2$] is expressed as

$$\begin{bmatrix} A_{11} & A_{12} \\ A_{21} & A_{22} \end{bmatrix} \begin{bmatrix} u_{1x} & u_{2x} \\ u_{1y} & u_{2y} \end{bmatrix} = \begin{bmatrix} v_{1x} & v_{2x} \\ v_{1y} & v_{2y} \end{bmatrix} \quad (1)$$

where, **A** is the affine transformation matrix. The positive definite symmetric matrix **P** defines the 2D strain tensor for deforming one cell into the other,

$$\mathbf{P} = \begin{bmatrix} 1+\epsilon_{xx} & \epsilon_{xy} \\ \epsilon_{xy} & 1+\epsilon_{yy} \end{bmatrix} \quad (2)$$

Because u_{1y}=v_{1y}=0, it leads the affine transformation matrix **A** as

$$\mathbf{A} = \begin{bmatrix} \frac{v_{1x}}{u_{1x}} & \frac{v_{2x}}{u_{2y}} - \frac{v_{1x}u_{2x}}{u_{1x}u_{2y}} \\ 0 & \frac{v_{2y}}{u_{2y}} \end{bmatrix} \quad (3)$$

From the polar decomposition of **A**, the rotation matrix **U** has a form as

$$\mathbf{U} = \begin{bmatrix} \cos(\phi) & -\sin(\phi) \\ \sin(\phi) & \cos(\phi) \end{bmatrix} \quad (4)$$

$$\phi = |\phi_a - \phi_b|/2 \quad (5)$$

$$\mathbf{P} = \boldsymbol{U}^{\boldsymbol{T}}\mathbf{A} \quad (6)$$

where, ϕ_a is the angle between the vectors $\mathbf{u}_1$ and $\mathbf{u}_2$, ϕ_b is the angle between the vectors $\mathbf{v}_1$ and $\mathbf{v}_2$.

We start modelling the MoS_2/PtS_2 heterogeneous interfaces using the Quantum Atomistix ToolKit (ATK2018.06) simulation tools[26]. The top and side views of the atomic geometries of the MoS_2/PtS_2 heterogeneous interfaces are shown in Figure 1(c) and 1(d). The parallel twisted MoS_2/PtS_2 heterogeneous interfaces have been constructed by stacking a pair of opposite super cells. All the calculations have been performed within the framework of density functional theory (DFT). We use the generalized gradient approximation (GGA) with the parametrization of Perdew-Burke-Ernzerhof (PBE), mesh cut-off energy of 100 Hartree and 12×12×1 k-points grid is used for the optimization calculations. To calculate the distance between two layers, we use the semi-empirical corrections by Grimme DFT-D2 model, which takes account the long-range vdW interaction[27]. A large vacuum spacing of at least 20 Å is added along the *c*-direction to avoid the interactions that arise while calculating the periodic boundary conditions. The structure is fully relaxed until the force on each atom becomes smaller than 0.01 eV/Å. In the electrical and optical properties simulation, we used the Heyd-Scuseria-Ernzerhof (HSE) method, which often leads to reasonable estimations for the bandgap and optical absorption [28]. Previous studies show that GW calculation gave higher bandgaps than HSE calculation for 2D materials [29]. For example, GW and HSE bandgaps for monolayer MoS_2 are 2.53 eV and 2.04 eV respectively, while the experiment result is about 1.80 eV [30]. Moreover, the HSE calculations are lower computationally expensive than the GW calculations. Thus, the band structure and optical properties are calculated by HSE calculation in this work.

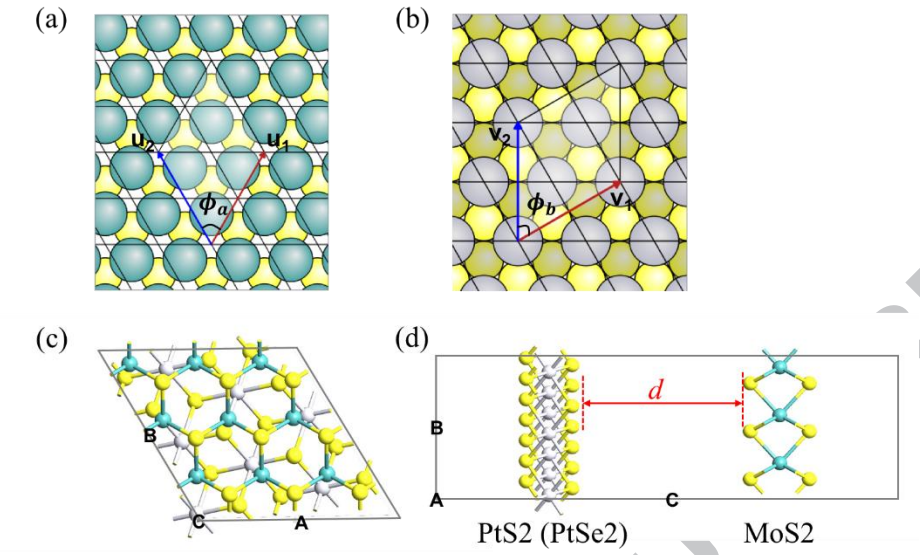

Figure 1. The select surface cell of MoS_2 (a) and PtS_2 (b). (c) and (d) show the top and side view of the atomic arrangement of the MoS_2/PtS_2 heterogeneous interfaces, d indicates the surface distance between two layers.

The initial stacking structure of MoS_2/PtS_2 heterogeneous interfaces has been constructed by a pair of oppositely skewed MoS_2 and PtS_2 supercells. When the rotation angle is 0^o, the MoS_2/PtS_2 heterogeneous interface belongs to 'C7' stacking. Different initial stacking configurations of the heterobilayers could generate different geometries for bilayers with the same rotation angle. In the prior research, 'C7', 'T', 'C27' and 'AA' stackings are four typical stacking configurations of TMDs heterogeneous [17, 31, 32]. The choice of stacking type to be analyzed was based on a two-step selection procedure. In the first step, we tried building four stacking types, and only two of them ('AA' and 'C7') can be built by the first principle software. Second, we used the criterion of the minimum mean absolute strains. For the 'AA' and 'C7' stackings, the lowest mean absolute strains on the MoS_2 and PtS_2 surfaces in the range of 0^o - 60^o rotation angles are 2.90% and 3.03%, which are higher than the mean absolute strains in 'C7' stacking (Table 1). Hence, our research about MoS_2/PtS_2 heterogeneous interface with different twisting angles is based on the 'C7' stacking. We calculated the mismatch strain of the MoS_2/PtS_2 heterogeneous interface with 0^o rotation angle by GLM. Our calculations show that the mean absolute strains on the MoS_2 or PtS_2 surfaces are 6.97% or 6.31% respectively, which possibly induces the instability of the original atom layers because of a big mismatch

strain. In prior studies, the mismatch strains were usually less 2%-3% and the biggest mismatch strain was 5% [18, 19, 33]. The twisting angles of 19.1°, 30.0 ° and 40.9° are analyzed below. At these angles the structure is stable while having a smaller cell size. Using the Generalized Lattice Match method, the calculated rotation angle (θ), lattice constant (*a*), mean absolute strain on the MoS_2 layer (ε) and surface distance between two layers (*d*) are listed in Table 1. For MoS_2/PtS_2 heterogeneous interfaces, the interface distance is about 3.41 Å, which is close to those of the van der Waals structure in references[17-19]. The change of interlayer distance in the twisting MoS_2/PtS_2 heterogeneous interfaces generates relatively weak effect, which is very close to recent DFT calculation results on TMDs and nTMDs heterogeneous interfaces[17-19]. To analyze the interlayer interaction in the heterogeneous interfaces, we calculate the binding energies (E_b) using following function

$$E_b = (E_{homobilayers} - E_{MoS_2} - E_{PtS_2})/N_{MoS_2} \quad (7)$$

where, $E_{homobilayers}$, E_{MoS_2} and E_{PtS_2} are the energy of the MoS_2/PtS_2 heterogeneous interfaces, monolayer MoS_2 and PtS_2, respectively. N_{MoS_2} is the number of MoS_2 units in the heterogeneous interfaces. The results of calculated binding energies are shown in the Table 1. The binding energy becomes higher with the increase of the rotation angle. The maximum binding energy of MoS_2/PtS_2 heterogeneous interface is -300.12 meV when the rotation angle is at 40.9°. This evolution is similar to the previous studies of the PtS_2 (PdS_2)/Graphene and Graphene/MoS_2 heterogeneous interfaces [18, 19].

Table 1. Rotation angle (θ), lattice constant (a), mean absolute strain (ε), surface distance between two layers (d) and binding energy (E_b) for MoS_2/PtS_2 heterogeneous interfaces.

θ (°)	*a* (Å)	$\mathcal{E}$	*d* (Å)	E_b (meV)
19.1	9.47	0.06%	3.41	-414.31
30.0	6.20	1.29%	3.41	-347.12
40.9	9.47	0.06%	3.42	-300.12

As shown in Figure 2, the band structures of the Brillouin zone of high symmetry points and projected density of states (PDOS) for three twisting angles of the MoS_2/PtS_2 heterogeneous interfaces have been calculated by the HSE hybrid functional. However, it has some limitations, especially when comparing a bulk

material with a 2D material. As the HSE functional does not discriminate between the different screening behaviors in the bulk as compared to a 2D layer[28]. Here we use an optimized range-separated hybrid functional, which often leads to reasonable estimates for the band gap and optical adsorption[28]. The energy bands originated from the PtS_2 and MoS_2 are marked by red dots and blue lines, respectively. Obviously, the valence band maximum (VBM) and conduction band minimum (CBM) are contributed by the MoS_2 and PtS_2, respectively. Moreover, the PDOS for each heterogeneous interfaces shows that the VBM has the contribution mainly from the Mo-*d* orbital and CBM has the contribution mainly from the orbital coupling of the S-*p* and Pt-*d* (Figure 2). In other words, the electron transition from Mo-*d* orbital to S-*p* and Pt-*d* orbitals occurs at the energy about 1 eV, which is the calculated bandgap. Upon increasing the rotation angle, the CBM and VBM shift. In the MoS_2/PtS_2 heterogeneous interfaces, the CBM shifts from a point between *K* and *G* (19.1^o and 30.0^o) to a point between *G* and *M* (40.9^o), while the VBM shifts from the *G* point (19.1^o) to the *K* point (30.0^o) then back to the *G* point (40.9^o). The bands transition of the CBM is a result of the band folding effect of the PtS_2 layer, while the transition of VBM is attributed to the band dispersion subject to the lattice strain of MoS_2 layer. Previous researches have shown that the band structure of the MoS_2 monolayer changed from direct to indirect bandgap with the increase of lateral strain[34]. As the rotation angle increases to 30^o, it is seen that a clear change of the MoS_2 bands from direct to indirect type due to the 1.29% deformation rate on the MoS_2 surface in the Table 1. As shown in Figure 3, we calculated the average charge density difference of the MoS_2/PtS_2 with 30.0^o rotation angle. A clear charge density decrease is shown in the interface between MoS_2 and PtS_2. The redistribution of the charges leads to the charge accumulation (blue isosurface) and depletion (red isosurface), which is a key reason of the interface charge repulsion. Moreover, this effect leads to the interface orbital hybridization and electron transition from MoS_2 layer to PtS_2 layer, which is accordance with the results of the PDOS (Figure 2).

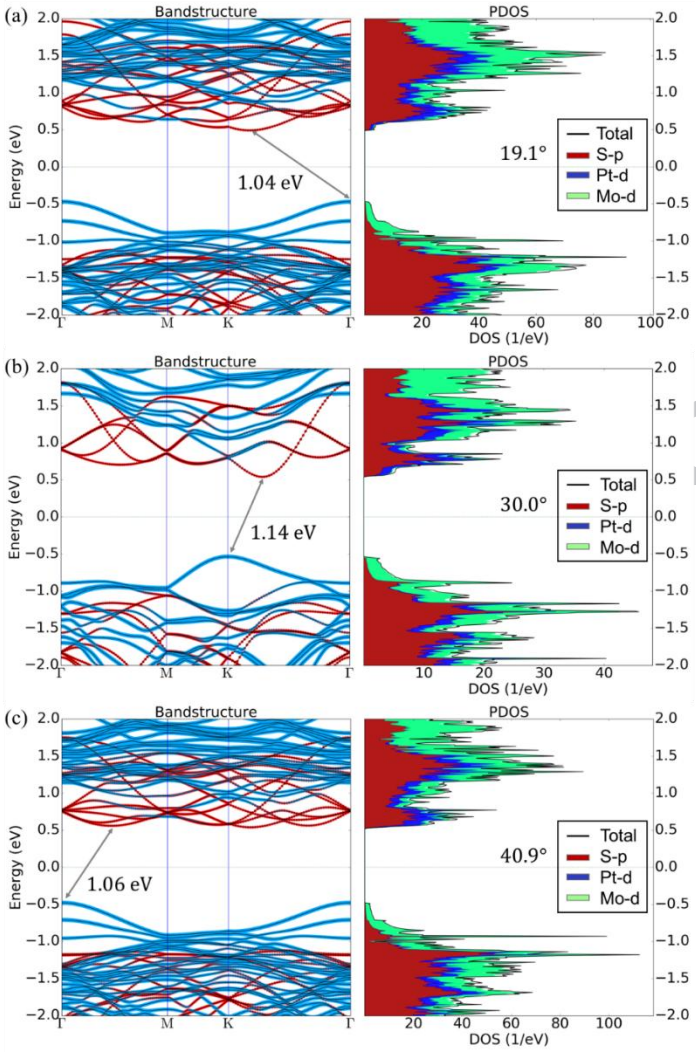

Figure 2. The computed band structures and PDOS of the MoS_2/PtS_2 heterogeneous interfaces with 19.1 ^{o} (a) 30.0 ^{o} (b) and 40.9 ^{o} (c) rotation angles.

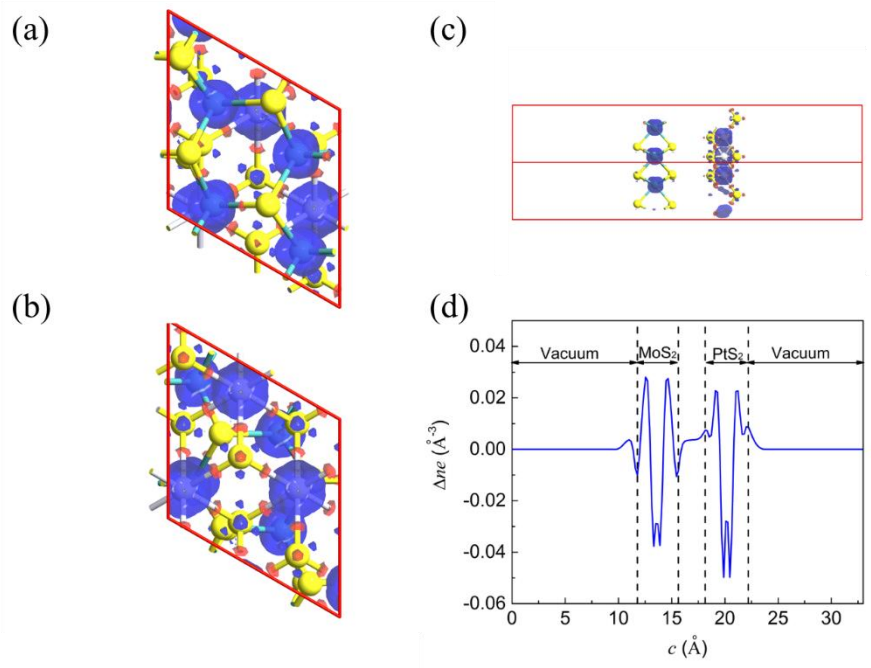

Figure 3. The computed MoS_2 surface view (a), PtS_2 surface view (b) side view (c) c-direction (d) charge density difference of the MoS_2/PtS_2 heterogeneous interfaces with 30.0^o rotation angles. Red and blue isosurface mark the depletion and aggregation of electrons, respectively.

3 Optical properties

We calculated the optical properties of twisted MoS_2/PtS_2 heterogeneous interfaces by using the HSE hybrid functional. The susceptibility tensor at a frequency ω can be expressed by the Kubo-Greenwood formula:

$$\chi_{ij}(\omega) = -\frac{e^2\hbar^4}{m^2\epsilon_0 V\omega^2}\sum_{nm}\frac{f(E_m)-f(E_n)}{E_{nm}-\hbar\omega-i\Gamma}\pi^i_{nm}\pi^j_{mn} \quad (8)$$

Where E_n, E_m and E_{nm} are the energy levels at states n, m and energy difference between the state n and m. f, Γ and V are the Fermi function, broadening and volume, respectively. π^i_{nm} is the i-th component of dipole matrix element between states n and m. ϵ_0, $\hbar$ and e are the vacuum dielectric constant, reduced Planck constant and elementary charge, respectively. The relative dielectric constant (ϵ_r) can be expressed as:

$$\epsilon_r(\omega) = (1 + \chi(\omega)) \quad (9)$$

The complex dielectric constant is related to the frequency ω as:

$$\epsilon(\omega) = \epsilon_0\epsilon_r(\omega) = \epsilon_1(\omega) + \epsilon_2(\omega) \quad (10)$$

The ϵ_0, ϵ_1 and ϵ_2 are the vacuum dielectric constant, real and imaginary parts of the complex dielectric constant, respectively.

From the Kramers-Kronig relations, the ϵ_1 and ϵ_2 can be expressed as:

$$\epsilon_1(\omega) = 1 + \frac{2}{\pi} A \int_0^{\infty} \frac{\omega' \epsilon_2(\omega')}{\omega'^2 - \omega^2} d\omega' \tag{11}$$

$$\epsilon_2(\omega) = -\frac{2\omega}{\pi} A \int_0^{\infty} \frac{\epsilon_1(\omega')}{\omega'^2 - \omega^2} d\omega' + \frac{\sigma_0}{\epsilon_0 \omega} \tag{12}$$

In equations (11) and (12), the σ_0 and A are the DC conductivity and the principal part of the integral. The extinction coefficient (κ) and refractive index (n) are related to the $\epsilon(\omega)$ through the $n + i\kappa = \sqrt{\epsilon(\omega)}$. From the terms of the real and imaginary parts of complex dielectric constant, the n and κ are given by:

$$n = \sqrt{\frac{\sqrt{\epsilon_1^2 + \epsilon_2^2} + \epsilon_1}{2}} \tag{13}$$

$$\kappa = \sqrt{\frac{\sqrt{\epsilon_1^2 + \epsilon_2^2} - \epsilon_1}{2}} \tag{14}$$

From the κ, the optical absorption coefficient (α_a) can be expressed as:

$$\alpha_a = 2\frac{\omega}{c}\kappa \tag{15}$$

where, c and ω are the speed and angular frequency of light. In the end, the reflectivity (r) is given by:

$$r = \frac{(1-n)^2 + \kappa^2}{(1+n)^2 + \kappa^2} \tag{16}$$

Figure 4 shows the real and imaginary parts of the complex dielectric constant for interlayer rotations on the MoS_2/PtS_2 heterogeneous interfaces. Here, we calculated the interlayer rotation angles at 19.1°, 30.0° and 40.9°. The values of the real part of the dielectric constant at the incident light energy of 0 eV for 19.1°, 30.0° and 40.9° rotation angles are 1.77, 2.25 and 1.77, respectively. Figure 4(b) shows that the peaks of imaginary parts of the complex dielectric constant appearing between photonic energy of 1.75 eV and 2.00 eV. Looking at the spectrums of the real and imaginary parts of the dielectric constant, the absolute value of peaks at 30.0° are considerably larger than at other rotation angles.

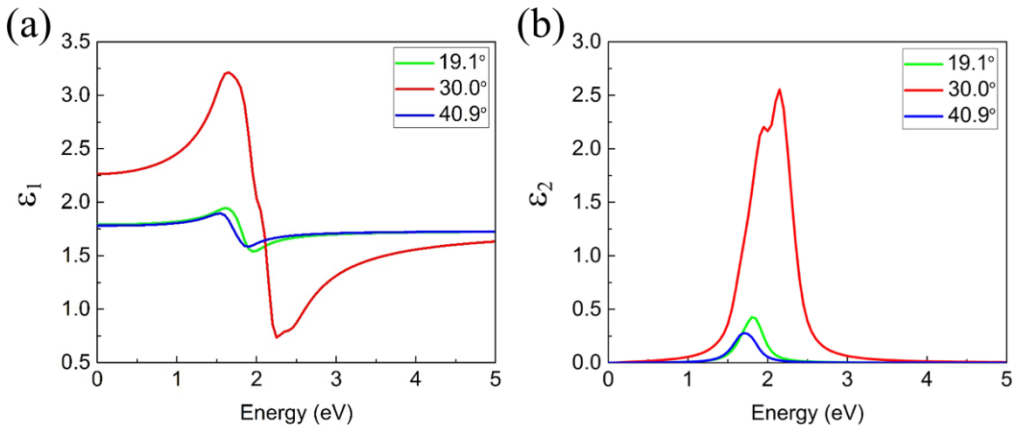

Figure 4. The real (a) and imaginary (b) parts of the complex dielectric constant for interlayer rotations on the MoS_2/PtS_2 heterogeneous interfaces.

Figure 5 shows the refractive index, extinction coefficient, reflectivity and absorption coefficient spectrums of the MoS_2/PtS_2 heterogeneous interfaces with 19.1°, 30.0° and 40.9° interlayer rotation angles. The refractive index curves (Figure 5(a)) show a minimum at photonic energy between 1.77 eV and 2.36 eV, while a maximum at around 1.55 eV. Moreover, the fluctuation ranges of the refractive index under 30.0° rotation angle is 0.85, which is 5.7 and 7.1 times higher than the 19.1° and 40.9° rotation angles. In Figure 5(b), the maximum of the extinction coefficient with 30.0° rotation angle is 0.91, which is 5.7 and 8.7 times higher than 19.1° and 40.9° rotation angles. The photonic energy of the peaks with 19.1°, 30.0° and 40.9° interlayer rotation angles are from 1.77 eV to 1.85 eV. Figure 5(c) plots the reflectivity curves varying with the photonic energy. The reflectivity curves have a similar evolution trend as the refractive index curves. The fluctuation range of reflectivity under 30.0° rotation angle is 0.15, which is 9.2 and 12.0 times higher than 19.1° and 40.9° rotation angles. Figure 5(d) shows the absorption index curves with the photon energy. The absorption index under 30.0° interlayer rotation angle is one order of magnitude more than other rotation angles at the same photonic energy. For the 30.0° interlayer rotation, the absorption coefficient of higher than 10^5 /cm is maintained between 1.90 eV and 2.35 eV (528-653 nm), which even displays high absorptions at visible light region. The optical properties of MoS_2/PtS_2 heterogeneous are attributed to the nature of the atomic orbitals, which comes from the band extreme of the material [24]. The heterostructure configurations for the 19.1 °, 30.0 ° and 40.9 ° rotation angles,

particularly the sizes of unit-cells are 48 atoms, 21 atoms, and 48 atoms respectively. Under the 30 ^{o} rotation angle, the MoS_2/PtS_2 heterogeneous structure possesses more energy band peaks in both conduction and valence zones. These additional band peaks facilitate the optical transition across the gap, which results in larger optical properties of MoS_2/PtS_2 heterogeneous under 30 ^{o} rotation angle.

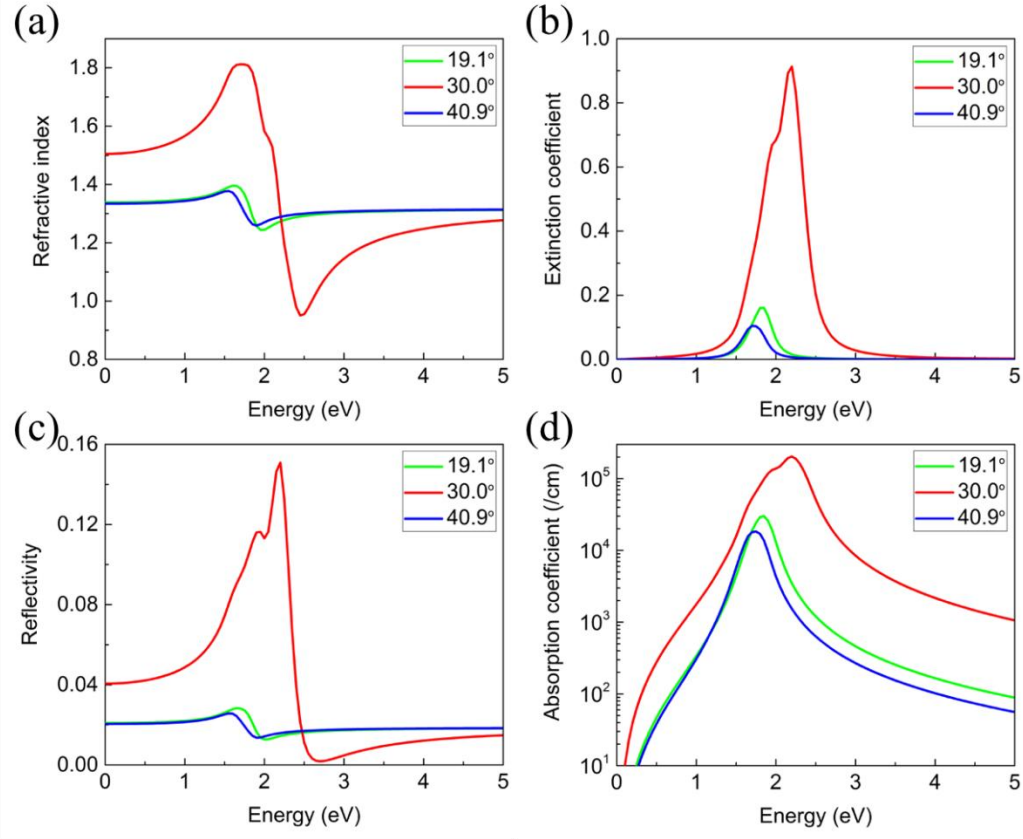

Figure 5. The refractive index (a), extinction coefficient (b), reflectivity (c) and absorption coefficient (d) spectrums of the MoS_2/PtS_2 heterogeneous interfaces.

We can interpret the relations among the refractive index, extinction coefficient, reflectivity, absorption coefficient, and dielectric constant by the Lorentz model, which is applicable to semiconductors[35]. In the Lorentz model, the atom with the electronic bond to the nucleus is analogues to a small mass bonded to a large mass by a spring. Assume the twisted heterostructure and the incident light to be a collection of damped harmonic oscillators with a characteristic vibrational frequency and the light frequency are ω_0 and ω, respectively. In the regime of the high absorption band ($\omega \approx \omega_0$), the imaginary part of the complex dielectric constant, extinction coefficient and absorption coefficient achieve the peak, the refractive index and real

part of the complex dielectric constant decrease with the increase of the photonic energy. In the regime of the low frequency ($\omega \ll \omega_0$), the imaginary part of the complex dielectric constant, extinction coefficient and absorption coefficient increase with the increase of the photonic energy, the refractive index and real part of the complex dielectric constant increase with the increase of the photonic energy. The material is transparent in this regime. In the regime of the high frequency ($\omega \gg \omega_0$), the imaginary part of the complex dielectric constant, extinction coefficient and absorption coefficient decrease with the increase of the photonic energy, while the refractive index increase with the increase of the photonic energy.

The strain-dependent absorption coefficient of the MoS_2/PtS_2 heterogeneous interface with 30.0^o rotation angle has been calculated and shown in Figure 6. The symmetrical biaxial external tensile deformation ranging between 0 and 5% is applied. The magnitude of strain is defined as $\Delta\varepsilon = (a - a_0)/a_0$, where a_0 and a are the equilibrium and strained lattice values, respectively. In the Figure 6, the observation reveals that the high absorption band shifts toward longer wavelengths. This red-shift is almost uniform with the increasing strain values. Essentially it is not only red-shift of the spectrum, the strain also introduces band broadening, which increases the absorption band by 350 nm (shown in Figure 6). The band broadening effect causes the high absorption being expanded to visible region. Table 2 shows the absorption coefficient and absorption wavelength of the MoS_2/PtS_2 heterogeneous interface compared with other heterogeneous materials. Obviously, the range of absorption wavelength of the MoS_2/PtS_2 is wider than other heterogeneous interfaces except for the Graphene/MoS_2 heterogeneous interface. However, the absorption coefficient of Graphene/MoS_2 is only from 1.0×10^4 /cm to 8.5×10^4 /cm, which is one order of magnitude lower than the MoS_2/PtS_2 heterogeneous interface. Although the absorption coefficient peak of GeSe/SnS and Phosphorene nanoflakes heterogeneous interfaces are higher than MoS_2/PtS_2 heterogeneous interface, the absorption bandwidth spans ultraviolet to visible light, which does not include near infrared. It is worth to highlight that under the 5% external tensile deformation, the high absorption band is from around 450 nm (visible light) to around 1050 nm (near infrared), which for the first time demonstrates high absorption at infrared region compared with prior investigations. Here DFT simulation did not consider excitonic binding energy of this

heterostructure, and the optical absorption spectrum corresponding to the excitonic effect in far-infrared is not shown. From the values of ground states bandgap and exciton binding energies, the excitons induced optical absorption band is far away from the ground states induced absorption, hence there will be less interaction / impact between two spectrums, which can be reasonably considered as extra absorption bands in very long wavelength regions.

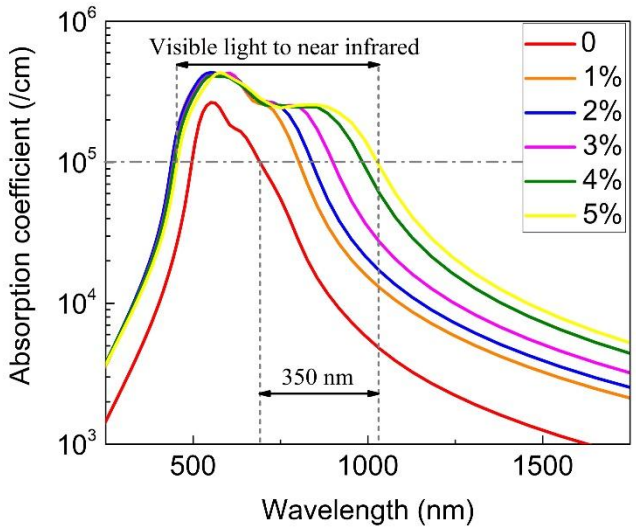

Figure 6. The absorption coefficient spectrums of the 30.0^o twisted MoS_2/PtS_2 heterogeneous interface under the biaxial tensile strains.

Table 2. Absorption coefficient and wavelength of different heterogeneous interfaces.

Heterogeneous interface	Absorption wavelength (nm)	Absorption coefficient (/cm)
Graphene/MoS_2[36]	150-1200	1.0×10^4-8.5×10^4
InSe/MoS_2[37]	300-800	No order
GaN/WS_2[38]	100-210	1.0×10^5-1.8×10^5
GaN/WSe_2[38]	100-200	1.0×10^5-1.4×10^5
Born phosphide/Blue phosphorus[39]	120-620	No order
GeSe/SnS[24]	50-600	1.0×10^5-9.0×10^5
C_2N/Sb[23]	177-310	1.0×10^5-1.2×10^5
Phosphorene nanoflakes[40]	248-496	1.0×10^5-7.0×10^5
MoS_2/PtS_2 (our results)	450-1050	1.0×10^5-3.5×10^5

4 Spain-orbit coupling effect

We calculated the electronic band structure and the dielectric constant taking into consideration Spin-orbit coupling (SOC) effect in the Figures 7. The bands are projected to spin up and down by red and blue lines, respectively. In order to provide a comparison, the bandgaps of the MoS_2/PtS_2 heterogeneous interfaces with 19.1^o, 30.0^o and 40.9^o rotation angles are calculated with and without SOC effect are shown in the Table 3. The indirect bandgap decreases by around 9.5 meV, for the 19.1^o rotation angle the main reason is that the spin orbit induce a light spitting (11.9 meV) of the CBM between *K* and *G* point, which causes the CBM to decrease. The VBM is nearly unaffected due to a small spin orbit spitting at *G* point. For the MoS_2/PtS_2 heterogeneous interface with 30.0^o, the bandgap decreases by about 50.0 meV due to a clear spin orbit spitting at VBM about 127.3 meV, while a slight spin orbit spitting at CBM about 10.6 meV. For the MoS_2/PtS_2 heterogeneous interface with 40.9^o, the main reason of the bandgap decreasing by around 9.6 meV is the spin orbit induced spitting of CBM between *G* point and *M* point (12.4 meV). Under the SOC effect, the values of the real part of the dielectric constant at the incident light energy of 0 eV for 19.1^o, 30.0^o and 40.9^o rotation angles increase by 0.07, 0.18 and 0.11, respectively. Moreover, the Figure 7(e) shows that the peaks of imaginary parts of the complex dielectric constant increase by 0.53, 0.51 and 0.74 appearing between photonic energy of 1.75 eV and 2.00 eV. The strain-dependent absorption coefficient of the MoS_2/PtS_2 heterogeneous interface with 30.0^o rotation angle has been calculated with the SOC effect in Figure 7(f). The main change is that the absorption band widening due to the mechanical strain decreases from 350 nm to 280 nm.

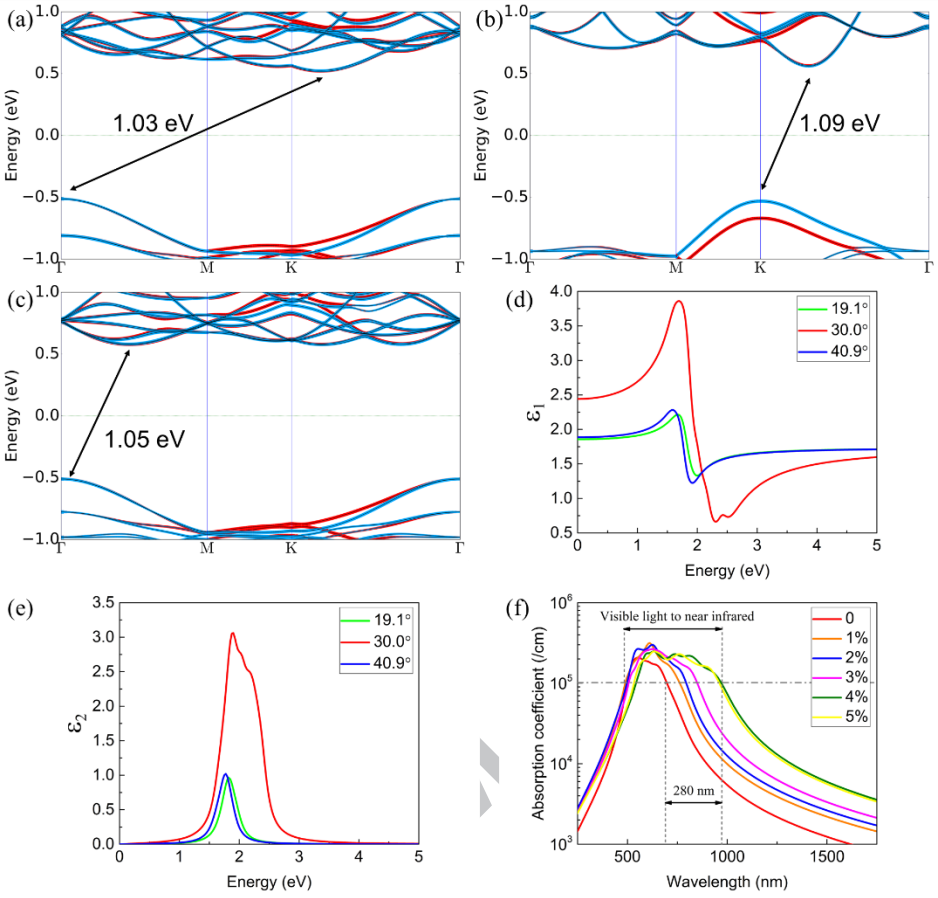

Figure7. The computed band structures with 19.1° (a) 30.0° (b) 40.9° (c) rotation angles, real (d), imaginary (e) parts of the complex dielectric constant and absorption coefficient spectrums with the 30.0° rotation angles under the biaxial tensile strains of the MoS_2/PtS_2 heterogeneous interfaces considering the SOC effect.

Table 3. Bandgap computed with and without SOC effect for MoS_2/PtS_2 heterogeneous interfaces.

	19.1°	30.0°	40.9°
Without SOC	1.04 eV	1.14 eV	1.06 eV
With SOC	1.03 eV	1.09 eV	1.05 eV

5 Conclusion

To summarize, *ab initio* simulations have been conducted to investigate the electronic and optical properties of the MoS_2/PtS_2 heterogeneous interfaces subject to various twisting angles. The structure, electronic and optical properties of MoS_2/PtS_2 heterogeneous interfaces have been optimized and subsequently simulated when subjecting to parallel twisting angles. Main conclusions are drawn that the peak

absolute values of the refractive index, extinction coefficient, reflectivity and absorption coefficient under 30.0^o rotation angle are far bigger than 19.1^o and 40.9^o rotation angles. In addition, under the 30.0^o twisting angle, the high absorption coefficient ($>10^5$/cm) of MoS_2/PtS_2 heterogeneous interface has a red-shift and a broadening effect with the tensile strain, from roughly 700 nm (0% external strain) to 1050 nm (5% external strain), in the meantime a significant band broadening effect of the high absorption band has been shown under tensile strains. Although there is no experimental research about applying strain on a twisted heterogeneous interface until now, the experiment demonstrating strain and twisted interlayer tuning electrical and optical properties of 2D transition metal dichalcogenides TMDs heterogeneous structures are proposed in some prior works [41, 42]. Therefore, theoretical research of applying strain on a twisted heterogeneous interface is important to explore the potential application in tunable optoelectronic devices.

Conflict of interest

There are no conflicts to declare.

Acknowledgements

Authors are grateful for funding by the China Scholarship Council (CSC). The authors would like to acknowledge the European Regional Development Fund (ERDF) for the funding of the Solar Photovoltaic Academic Research Consortium (SPARC II) which supported this research.

References

[1] K.S. Novoselov, A. Mishchenko, A. Carvalho, A.H.C. Neto, 2D materials and van der Waals heterostructures, Science, 353 (2016).

[2] L.J. Li, Y. Zhang, Controlling the luminescence of monolayer MoS2 based on the piezoelectric effect, Nano Res., 10 (2017) 2527-2534.

[3] Q.H. Wang, K. Kalantar-Zadeh, A. Kis, J.N. Coleman, M.S. Strano, Electronics and optoelectronics of two-dimensional transition metal dichalcogenides, Nat. Nanotechnol., 7 (2012) 699-712.

[4] X.P. Fu, F.F. Li, J.F. Lin, Y.B. Gong, X.L. Huang, Y.P. Huang, B. Han, Q. Zhou, T. Cui, Pressure-Dependent Light Emission of Charged and Neutral

Excitons in Monolayer MoSe2, J. Phys. Chem. Lett., 8 (2017) 3556-3563.
[5] Y. Cao, V. Fatemi, S. Fang, K. Watanabe, T. Taniguchi, E. Kaxiras, P. Jarillo-Herrero, Unconventional superconductivity in magic-angle graphene superlattices, Nature, 556 (2018) 43-+.
[6] S. Deng, L.J. Li, M. Li, Stability of direct band gap under mechanical strains for monolayer MoS2, MoSe2, WS2 and WSe2, Physica E-Low-Dimensional Systems & Nanostructures, 101 (2018) 44-49.
[7] S. Deng, Y. Zhang, L.J. Li, Strain Magnitude and Direction Effect on the Energy Band Structure of Hexagonal and Orthorhombic Monolayer MoS2, IEEE Trans. Nanotechnol., 17 (2018) 419-423.
[8] S.D. Guo, Biaxial strain tuned thermoelectric properties in monolayer PtSe2, J. Mater. Chem. C, 4 (2016) 9366-9374.
[9] Y.D. Zhao, J.S. Qiao, Z.H. Yu, P. Yu, K. Xu, S.P. Lau, W. Zhou, Z. Liu, X.R. Wang, W. Ji, Y. Chai, High-Electron- Mobility and Air-Stable 2D Layered PtSe2 FETs, Adv. Mater., 29 (2017).
[10] A.D. Oyedele, S.Z. Yang, L.B. Liang, A.A. Puretzky, K. Wang, J.J. Zheng, P. Yu, P.R. Pudasaini, A.W. Ghosh, Z. Liu, C.M. Rouleau, B.G. Sumpter, M.F. Chisholm, W. Zhou, P.D. Rack, D.B. Geohegan, K. Xiao, PdSe2: Pentagonal Two-Dimensional Layers with High Air Stability for Electronics, J. Am. Chem. Soc., 139 (2017) 14090-14097.
[11] M.A. ElGhazali, P.G. Naumov, H. Mirhosseini, V. Suss, L. Muchler, W. Schnelle, C. Felser, S.A. Medvedev, Pressure-induced superconductivity up to 13.1 K in the pyrite phase of palladium diselenide PdSe2, Phys. Rev. B, 96 (2017) 060509.
[12] P. Miro, M. Ghorbani-Asl, T. Heine, Two Dimensional Materials Beyond MoS2 : Noble-Transition-Metal Dichalcogenides, Angew Chem Int Edit, 53 (2014) 3015-3018.
[13] S. Deng, L.J. Li, Y. Zhang, Strain modulated electronic, mechanical, and optical properties of the monolayer PdS2, PdSe2, and PtSe2 for tunable devices, ACS Appl. Nano Mater., 1 (2018) 1932-1939.
[14] Y. Cao, V. Fatemi, A. Demir, S. Fang, S.L. Tomarken, J.Y. Luo, J.D. Sanchez-Yamagishi, K. Watanabe, T. Taniguchi, E. Kaxiras, R.C. Ashoori, P. Jarillo-Herrero, Correlated insulator behaviour at half-filling in magic-angle

graphene superlattices, Nature, 556 (2018) 80-+.
[15] W. Yao, E.Y. Wang, C.H. Bao, Y.O. Zhang, K.A. Zhang, K.J. Bao, C.K. Chan, C.Y. Chen, J. Avila, M.C. Asensio, J.Y. Zhu, S.Y. Zhou, Quasicrystalline 30 degrees twisted bilayer graphene as an incommensurate superlattice with strong interlayer coupling, Proc. Natl. Acad. Sci. U.S.A., 115 (2018) 6928-6933.
[16] S.J. Ahn, P. Moon, T.-H. Kim, H.-W. Kim, H.-C. Shin, E.H. Kim, H.W. Cha, S.-J. Kahng, P. Kim, M. Koshino, Y.-W. Son, C.-W. Yang, J.R. Ahn, Dirac electrons in a dodecagonal graphene quasicrystal, Science, (2018).
[17] N. Lu, H.Y. Guo, Z.W. Zhuo, L. Wang, X.J. Wu, X.C. Zeng, Twisted MX2/MoS2 heterobilayers: effect of van der Waals interaction on the electronic structure, Nanoscale, 9 (2017) 19131-19138.
[18] Z.L. Wang, Q. Chen, J.L. Wang, Electronic Structure of Twisted Bilayers of Graphene/MoS2 and MoS2/MoS2, J. Phys. Chem. C, 119 (2015) 4752-4758.
[19] S.Y. Hou, L.H. Han, L.Y. Wu, R.G. Quhe, P.F. Lu, Robust quasi-ohmic contact against angle rotation in noble transition-metal-dichalcogenide/graphene heterobilayers, Rsc Advances, 7 (2017) 45896-45901.
[20] K. Wang, B. Huang, M. Tian, F. Ceballos, M.W. Lin, M. Mahjouri-Samani, A. Boulesbaa, A.A. Puretzky, C.M. Rouleau, M. Yoon, H. Zhao, K. Xiao, G. Duscher, D.B. Geohegan, Interlayer Coupling in Twisted WSe2/WS2 Bilayer Heterostructures Revealed by Optical Spectroscopy, ACS Nano, 10 (2016) 6612-6622.
[21] C.D. Zhang, C.P. Chuu, X.B. Ren, M.Y. Li, L.J. Li, C.H. Jin, M.Y. Chou, C.K. Shih, Interlayer couplings, Moire patterns, and 2D electronic superlattices in MoS2/WSe2 hetero-bilayers, Sci. Adv., 3 (2017).
[22] F. Ning, D. Wang, Y.X. Feng, L.M. Tang, Y. Zhang, K.Q. Chen, Strong interfacial interaction and enhanced optical absorption in graphene/InAs and MoS2/InAs heterostructures, J. Mater. Chem. C, 5 (2017) 9429-9438.
[23] X.L. Wang, R. Quhe, W. Cui, Y.S. Zhi, Y.Q. Huang, Y.H. An, X.Q. Dai, Y.N. Tang, W.G. Chen, Z.P. Wu, W.H. Tang, Electric field effects on the electronic and optical properties in C2N/Sb van der Waals heterostructure, Carbon, 129

(2018) 738-744.
[24] C.X. Xia, J. Du, W.Q. Xiong, Y. Jia, Z.M. Wei, J.B. Li, A type-II GeSe/SnS heterobilayer with a suitable direct gap, superior optical absorption and broad spectrum for photovoltaic applications, J Mater Chem A, 5 (2017) 13400-13410.
[25] L. Jelver, P.M. Larsen, D. Stradi, K. Stokbro, K.W. Jacobsen, Determination of low-strain interfaces via geometric matching, Phys. Rev. B, 96 (2017).
[26] Atomistix ToolKit (ATK), https://quantumwise.com/. .
[27] S. Grimme, Semiempirical GGA-type density functional constructed with a long-range dispersion correction, J. Comput. Chem., 27 (2006) 1787-1799.
[28] D. Luftner, S. Refaely-Abramson, M. Pachler, R. Resel, M.G. Ramsey, L. Kronik, P. Puschnig, Experimental and theoretical electronic structure of quinacridone, Phys. Rev. B, 90 (2014).
[29] S. Haastrup, M. Strange, M. Pandey, T. Deilmann, P.S. Schmidt, N.F. Hinsche, M.N. Gjerding, D. Torelli, P.M. Larsen, A.C. Riis-Jensen, J. Gath, K.W. Jacobsen, J.J. Mortensen, T. Olsen, K.S. Thygesen, The Computational 2D Materials Database: high-throughput modeling and discovery of atomically thin crystals, 2d Materials, 5 (2018).
[30] K.F. Mak, C. Lee, J. Hone, J. Shan, T.F. Heinz, Atomically thin MoS_2: a new direct-gap semiconductor, Phys Rev Lett, 105 (2010) 136805.
[31] K. Kosmider, J. Fernandez-Rossier, Electronic properties of the MoS2-WS2 heterojunction, Phys. Rev. B, 87 (2013).
[32] N. Lu, H.Y. Guo, L. Li, J. Dai, L. Wang, W.N. Mei, X.J. Wu, X.C. Zeng, MoS2/MX2 heterobilayers: bandgap engineering via tensile strain or external electrical field, Nanoscale, 6 (2014) 2879-2886.
[33] Y. Matsushita, H. Nishi, J. Iwata, T. Kosugi, A. Oshiyama, Unfolding energy spectra of double-periodicity two-dimensional systems: Twisted bilayer graphene and MoS2 on graphene, Phy Rev Mater, 2 (2018).
[34] E. Scalise, M. Houssa, G. Pourtois, V.V. Afanas'ev, A. Stesmans, Strain-induced semiconductor to metal transition in the two-dimensional honeycomb structure of MoS2, Nano Research, 5 (2012) 43-48.
[35] F. W, Optical Properties of Solids, Academic Press, 1972.

[36] X.T. Hua, X.G. Ma, J.S. Hu, H. He, G.W. Xu, C.Y. Huang, X.B. Chen, Controlling electronic properties of MoS2/graphene oxide heterojunctions for enhancing photocatalytic performance: the role of oxygen, Phys. Chem. Chem. Phys., 20 (2018) 1974-1983.
[37] J. Zhang, X.Y. Lang, Y.F. Zhu, Q. Jiang, Strain tuned InSe/MoS2 bilayer van der Waals heterostructures for photovoltaics or photocatalysis, Phys. Chem. Chem. Phys., 20 (2018) 17574-17582.
[38] R.S. Meng, J.K. Jiang, Q.H. Liang, Q. Yang, C.J. Tan, X. Sun, X.P. Chen, Design of graphene-like gallium nitride and WS2/WSe2 nanocomposites for photocatalyst applications, Sci China Mater, 59 (2016) 1027-1036.
[39] Y. Mogulkoc, M. Modarresi, A. Mogulkoc, B. Alkan, Electronic and optical properties of boron phosphide/blue phosphorus heterostructures, Phys. Chem. Chem. Phys., 20 (2018) 12053-12060.
[40] W. Hu, J.L. Yang, Two-dimensional van der Waals heterojunctions for functional materials and devices, J. Mater. Chem. C, 5 (2017) 12289-12297.
[41] Y.M. He, Y. Yang, Z.H. Zhang, Y.J. Gong, W. Zhou, Z.L. Hu, G.L. Ye, X. Zhaug, E. Bianco, S.D. Lei, Z.H. Jin, X.L. Zou, Y.C. Yang, Y. Zhang, E.Q. Xie, J. Lou, B. Yakobson, R. Vajtai, B. Li, P. Ajayan, Strain-Induced Electronic Structure Changes in Stacked van der Waals Heterostructures, Nano Lett., 16 (2016) 3314-3320.
[42] A.M. van der Zande, J. Kunstrnann, A. Chernikov, D.A. Chenet, Y.M. You, X.X. Zhang, P.Y. Huang, T.C. Berkelbach, L. Wang, F. Zhang, M.S. Hybertsen, D.A. Muller, D.R. Reichman, T.F. Heinz, J.C. Hone, Tailoring the Electronic Structure in Bilayer Molybdenum Disulfide via Interlayer Twist, Nano Lett., 14 (2014) 3869-3875.

Study on electronic and optical properties of the twisted and strained MoS_2/PtS_2 heterogeneous interfaces

Shuo Deng[1, 3], Yan Zhang[2*], and Lijie Li[3*]

[1]School of Logistic Engineering, Wuhan University of Technology, Wuhan 430070, China

[2]School of Physics, University of Electronic Science and Technology of China, Chengdu 610054, China

[3]College of Engineering, Swansea University, Swansea SA1 8EN, UK

[*]Emails: zhangyan@uestc.edu.cn, L.Li@swansea.ac.uk

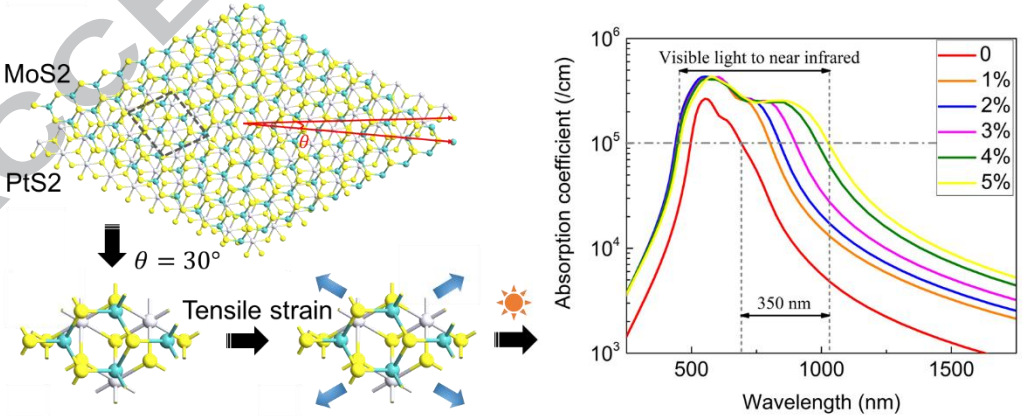

Study on electronic and optical properties of the twisted and strained MoS_2/PtS_2 heterogeneous interface

Shuo Deng[1, 3], Yan Zhang[2*], and Lijie Li[3*]

[1]School of Logistic Engineering, Wuhan University of Technology, Wuhan 430070, China

[2]School of Physics, University of Electronic Science and Technology of China, Chengdu 610054, China

[3]College of Engineering, Swansea University, Swansea SA1 8EN, UK

[*]Emails: zhangyan@uestc.edu.cn, L.Li@swansea.ac.uk

Highlights:

1. 2D MoS_2/PtS_2 heterogeneous interface has been simulated using DFT.
2. Twisting and strain effects are considered in the simulation.
3. Optical absorption spectrum has been found to be widened by twisting and strain.
4. Optical absorption peak has been significantly increased for certain twisting angles.